The relativistic layer-resolved electronic structure and photoemission of the adsorbate system Xe/Pt(111)

1994 J. Phys.: Condens. Matter 6 1913

(http://iopscience.iop.org/0953-8984/6/10/010)

J. Phys.: Condens. Matter 6 (1994) 1913–1926. Printed in the UK

The relativistic layer-resolved electronic structure and photoemission of the adsorbate system Xe/Pt(111)

J Henk and R Feder

Theoretische Festkörperphysik, Universität Duisburg, D-47048 Duisburg, Germany

Received 11 November 1993

Abstract. For the $(\sqrt{3} \times \sqrt{3})$R30° commensurate physisorption system Xe/Pt(111), the $k_{\parallel}$-, layer- and double-group-symmetry-resolved density of states (LDOS) as well as spin-resolved normal photoemission spectra for circularly and linearly polarized light have been calculated by means of a fully relativistic Green function formalism. Comparison with the LDOS obtained for an isolated Xe monolayer shows that the m_j splitting of the $5p_{3/2}$-derived states of the Xe adsorbate is almost exclusively due to the lateral interaction within the Xe layer. In contrast, Pt-derived features are strongly determined by the Xe overlayer via 'surface umklapp': firstly, electronic states localized in the two topmost Pt monolayers; and secondly, photoemission features originating from umklapped Pt bulk initial states. For circularly polarized light, we obtain very good agreement with experiment with regard to peak positions and sign of the spin polarization. Substantial discrepancies in absolute polarization values are ascribed to Auger-like electron–hole processes and call for an extension of our photoemission theory to incorporate these additional excitation channels. For linearly s-polarized light, the calculated spin polarization spectra depend very strongly on the lateral position of the Xe layer relative to the substrate.

1. Introduction

Rare-gas physisorption systems have been extensively studied experimentally (see, for example, Schönhense *et al* 1985, Kessler *et al* 1990, Heinzmann 1990 and references therein) by spin-resolved photoemission using circularly polarized synchrotron radiation. This is a powerful technique for obtaining, from spin–orbit coupling and relativistic dipole selection rules, detailed information on the electronic structure of (even non-magnetic) crystals and their surfaces (see reviews by Feder 1985, Kirschner 1985 and Heinzmann 1990, and representative papers by Tamura *et al* 1989, Schneider *et al* 1989, Stoppmanns *et al* 1991, Tamura and Feder 1991a, b, Halilov *et al* 1993a, b and references therein). However, apart from an early simple model calculation by Feder (1978), there are no theoretical studies of spin-resolved photoemission on rare-gas adsorption systems.

In the present work, we investigate in detail, as a typical case, Xe forming a commensurate $(\sqrt{3} \times \sqrt{3})$R30° overlayer on Pt(111). The electronic structure is characterized by the layer-, double-group-symmetry- and $k_{\parallel}$-resolved density of states, which we calculate by means of a recently developed fully relativistic Green function formalism (Halilov *et al* 1993, Tamura and Feder 1989). We thus find that the Xe overlayer, while electronically speaking almost identical with a hypothetical 'stand-alone' monolayer has, by virtue of surface umklapp processes, a rather profound effect on the substrate, in which it generates numerous surface states and resonances. Simultaneously, we apply a fully relativistic 'one-step-model' photoemission theory of the layer-KKR type, which is a generalized version (Halilov *et al* 1993, Tamura and Feder 1991a, b) of the

0953-8984/94/101913+14$19.50

formalism developed by Ackermann and Feder (1985) (see also ch. 4 of Feder 1985). The calculated spin-resolved spectra are found to agree well with their experimental counterparts (Schönhense *et al* 1985).

In section 2, we briefly recall the theoretical formalism, introduce a slight generalization allowing for a separate inner potential in the overlayer and describe the potential model specific for Xe/Pt(111). Section 3 is devoted to the geometrical structure of Xe/Pt(111). Our calculated results for the layer-resolved density of states and spin-resolved photoemission by circularly and linearly polarized light are presented and discussed in sections 4–6.

2. Theory

Our numerical calculations are based on a fully relativistic Green function formalism for semi-infinite crystalline systems, which yields layer- and double-group-symmetry-projected densities of states (Tamura and Feder 1989) as well as spin-resolved photoemission intensities (Tamura and Feder 1991a, b and references therein). A detailed presentation, including an extension to handle several atoms in the two-dimensional unit cell, has recently been given by Halilov *et al* (1993). The Green function treatment of the initial state allows, in contrast to an earlier Bloch wave treatment, an *a priori* incorporation of the hole lifetime in photoemission and a convenient determination of electronic surface states.

The effective quasi-particle potential is taken in the muffin-tin approximation. Its complex uniform part, the inner potential, includes energy-dependent self-energy corrections. In the absence of first-principles knowledge of the latter, we model the inner potential by parameters the values of which have to be verified *ex post facto* by the agreement between calculated and measured photoemission spectra. While for metal overlayers on a metallic substrate the inner potential of the overlayer can roughly be assumed to be the same as in the bulk (Stoppmanns *et al* 1991), it has quite different values, both in real and imaginary parts, for a rare-gas overlayer. The transition between the substrate and overlayer is taken as an abrupt step barrier modelled as refracting but non-reflecting. Its position in the region from the overlayer internuclear plane to the first substrate internuclear plane is taken as an adjustable parameter, for which we find an optimal value of 1.05 Å above the first substrate plane, i.e. 1/4 of the Xe–Pt interlayer distance of 4.2 Å (see section 3). For the real part of the inner potential of Pt we use $V_{0r}(\mathrm{Pt}) = 14.75\,\mathrm{eV}$ for the lower (occupied) states and $14.75\,\mathrm{eV} - 0.12(E - E_F)$ for the upper states (energies in eV), where E_F denotes the Fermi energy and $E > E_F$. For the imaginary part we take for Pt energy-dependent forms increasing (in absolute value) away from E_F as $V_{0i}(\mathrm{Pt}) = 0.025(E - E_F)$ for the lower and as $0.04(E - E_F)^{1.25}$ for the upper states. For Xe, we find $V_{0r}(\mathrm{Xe}) = 6.61\,\mathrm{eV}$ for the lower states. For the upper states, it is reduced to 4.61 eV. We note that this real self-energy correction of 2.0 eV is much smaller than the value of 4.15 eV found for bulk Xe (Halilov *et al* 1993b). The imaginary potential parts for Xe, because of its rare gas nature, are substantially smaller than for Pt. We choose $V_{0i}(\mathrm{Xe}) = 0.01(E - E_F)$ for the lower and −0.05 eV for the upper states.

As ion-core potentials we take for Pt a standard bulk potential obtained by a self-consistent LMTO calculation with the Hedin–Lundqvist exchange-correlation approximation (Hedin and Lundqvist 1971) and for Xe a recent self-consistent LMTO bulk potential (Halilov *et al* 1993b).

The surface potential barrier is simply taken as a refracting step, which is assumed to be reflecting for the lower states (for which there is indeed total internal reflection, as their energy is below the vacuum level) and, drawing upon LEED experience, to be non-reflecting for the upper states.

3. Surface geometry

In order to determine the geometrical structure of Xe/Pt(111) we have performed a detailed analysis of spin polarized low-energy electron diffraction (SPLEED) intensities. The questions upon which we focus are the lateral position of the Xe atoms with respect to the Pt substrate and the distance of the Xe layer from the outermost Pt layer. Furthermore, a comparison of theory with experiment determines the complex inner potentials of both Xe and Pt. Although these are obtained for higher energies, they provide clues to the respective values at lower energies as needed for the final states in the photoemission calculations.

The Xe atoms may be expected to occupy three types of lateral position with respect to the Pt layers. The so-called FCC-type overlayers continue the stacking sequence of the substrate ($\cdots$ABCABCA), whereas HCP-type overlayers show the stacking sequence $\cdots$ABCABCB. Overlayers in the on-top position have $\cdots$ABCABCC. All these lateral positions conserve the C_{3v} symmetry of the substrate. The distance in the direction normal to the surface has been varied from 3.2–5.2 Å.

Our calculated intensity and asymmetry profiles have been compared to the corresponding experimental data of Hilgers *et al* (1991) and Potthoff (1991). For the structure determination we focused on intensity and asymmetry against polar angle curves for the specular beam and the (1/3, 1/3) beam at energies 52 and 64 eV.

Our analysis essentially confirms the results obtained by Potthoff (1991) and Hilgers *et al* (1991). Since detailed comparisons of SPLEED spectra have been presented by these authors, we only briefly state our main results. The best overall agreement between theory and experiment is obtained for a vertical distance of $d_{\mathrm{Xe-Pt}} = 4.2$ Å. FCC- and HCP-adsorption sites can be clearly distinguished in theory. However, some structures in the measured asymmetry profiles are better reproduced by FCC-type overlayers, others by HCP-type overlayers. Therefore, we conclude that in experimental reality there are simultaneously domains of both types. The on-top position of the Xe atoms can be completely ruled out. The refracting but non-reflecting step barrier, which models the transition of the inner potential between substrate and adsorbate, is placed 1.05 Å above the topmost Pt internuclear plane, which corresponds to 25% of the Xe–Pt interlayer spacing. We note that the influence of this barrier position is stronger in photoemission than in SPLEED, because the Pt-derived initial-state wavefunctions (with energies below the Fermi level) are strongly damped in the Xe layer. The effective width of the latter is therefore more important.

4. Layer-resolved density of states

In this section, we focus on the electronic structure of the commensurate physisorption system $\sqrt{3} \times \sqrt{3}$R30°-Xe/Pt(111). As a prerequisite for interpreting our results we show in figure 1 the reciprocal-space geometry, i.e. the first (two-dimensional) surface Brillouin zone (SBZ) of this system in relation to that of the clean Pt(111) surface. In particular, we point out that the $\overline{\mathrm{K}}$-points of the 1×1 SBZ (denoted by $\overline{\mathrm{K}}_{1\times1}$ in figure 1) are equivalent to the $\overline{\Gamma}$-point of the SBZ of the overlayer system ('umklapp' by a surface reciprocal lattice vector).

In order to make features more visible and to facilitate their interpretation, we have calculated the layer density of states (LDOS) using a constant small value (0.05 eV) for the imaginary potential part. As is seen in figure 2, the LDOS at the $\overline{\Gamma}$-point ($k_{\parallel} = 0$) in the Xe layer consists almost exclusively of three peaks of double-group symmetry types Λ_6 and Λ_{4+5}. The lowest one corresponds to the $5p_{1/2}$ level of atomic Xe and the upper two

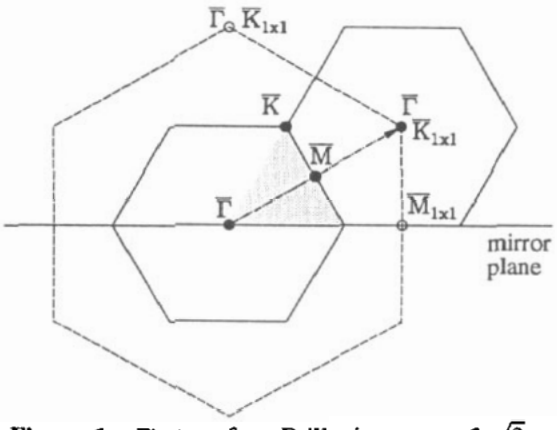

Figure 1. First surface Brillouin zones of $\sqrt{3} \times \sqrt{3}$R30°-Xe/Pt(111) (full lines) (with the irreducible part represented by the shaded area) and Pt(111) (broken lines). High symmetry points are indicated by full and open circles, respectively. The $\overline{K}$-points of the 1×1 SBZ (denoted by $\overline{K}_{1\times1}$), i.e. the corners of the broken hexagon, correspond to $\overline{\Gamma}$-points of the overlayer SBZ. Additionally, the trace of a mirror plane normal to the surface is shown.

are $m_j = 1/2$ and $m_j = 3/2$ partners arising from the atomic $5p_{3/2}$ level due to lateral interaction within the Xe layer. Amongst the various conceivable mechanisms for splitting the $5p_{3/2}$ level (see, for example, Waclawski and Herbst 1975), which lead to different relative ordering of the sublevels, this particular one has been singled out by Scheffler *et al* (1979) and substantiated by a spin-resolved photoemission experiment (Schönhense *et al* 1985). We have corroborated this interpretation by further calculations: for FCC- and HCP-type stacking of the Xe layer, upon changing the Xe–Pt interlayer distance and even when leaving the substrate (i.e. taking a stand-alone Xe monolayer), we obtain practically the same LDOS. The influence of the substrate on the electronic structure of the Xe layer is thus very small, as one would expect for a rare-gas adsorbate.

In the first Pt layer, the LDOS exhibits a wealth of sharp structures labelled S_1 to S_8. In order to understand these, we consider the bulk band structure of clean Pt along $\Gamma(\Lambda)$L (the bottom panel of figure 2). In addition to the usual Λ_6 and Λ_{4+5} bands of Pt, we show (by chain curves) bands backfolded to Γ from the $\overline{K}_{1\times1}$-points by the shortest adsorbate reciprocal lattice vector. These bands are found to be degenerate with respect to states of Λ_6 and Λ_{4+5} symmetry. Returning to the LDOS peaks S_1 to S_8, it is seen that they occur at energies in band gaps of the backfolded bulk band structure. This identifies them as surface states associated with 'surface umklapp'. From the just-mentioned degeneracy it is understandable that they can contain contributions of both double-group symmetry types, with the relative weights even changing from the first to the second Pt layer (see, for example, S_1 and S_3). The absence of these Pt surface states in the Xe layer is easily understood: since their energies are below the real part of the Xe inner potential, their wavefunctions can hardly extend into the Xe layer. In contrast, the weak feature I_1 near -0.2 eV is present in both the Xe and the first Pt layer. We interpret it as an interface state analogous to the one found by Stoppmanns *et al* (1991) for Au/Pt(111). The interface state and the Pt surface states are practically the same for FCC- and HCP-type stacking of the Xe layer.

To pursue the Pt surface states somewhat further, we have also calculated the LDOS for clean Pt(111) (see figure 3) for $k_\parallel$ at $\overline{\Gamma}$ (full curves) and $\overline{K}_{1\times1}$ (broken curves). While at $\overline{\Gamma}$ there is only the already known surface feature near 0.5 eV above the Fermi level (see Tamura and Feder 1989), there are nine surface features (labelled $S'_0, \ldots, S'_9$) at $\overline{K}_{1\times1}$. S'_6 to S'_9 are seen to correspond, with a right-shift increasing with decreasing binding energy,

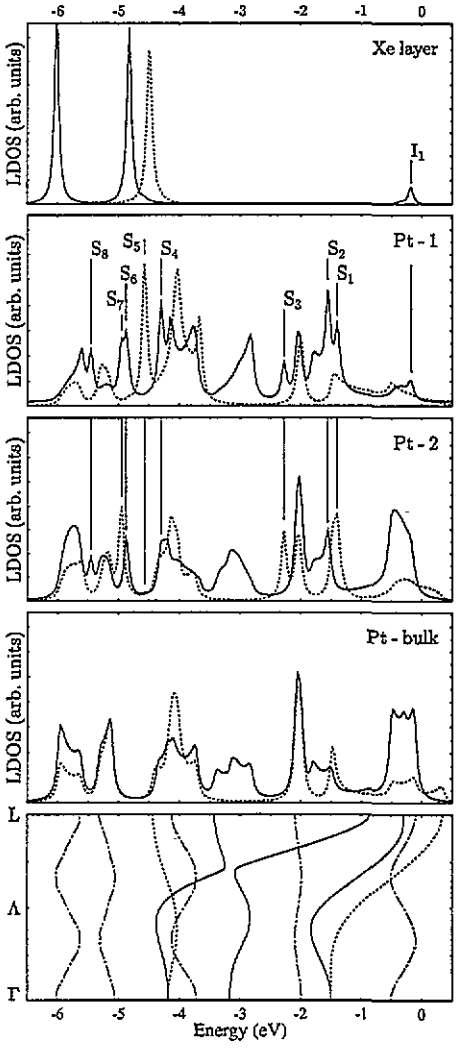

Figure 2. $\sqrt{3} \times \sqrt{3}$R30°-Xe/Pt(111): layer density of states for $k_\parallel = 0$ for Xe-adsorbate layer (top panel), the two outermost Pt layers (second and third panels) and a bulk Pt layer (fourth panel) resolved with respect to double-group symmetry types Λ_6 and Λ_{4+5} (full and broken curves). All LDOS panels have the same ordinate scale. Pt-derived surface states are denoted by $S_1, \ldots, S_8$, the Xe/Pt interface state by I_1. The corresponding bulk band structure (bottom panel) consists of the bands along Γ–Λ–L of usual bulk Pt (full and broken curves) and those backfolded from the $\overline{\mathrm{K}}_{1\times1}$-points (chain curves). The energy zero is the Fermi level.

to S_5 to S_8 on Xe/Pt (figure 2). S_4 has merged into the bulk band and is therefore no longer present. In the bulk band gap around -3 eV there are two new surface states, S_4' and S_5', which in fact have recently been observed experimentally by Di *et al* (1992). In the gap around -1 eV there are two surface features, S_1' and S_2', as on Xe/Pt, but at different energies. The observed differences between the Pt surface states on clean Pt and on Xe/Pt are plausible: firstly, surface states depend sensitively upon the details of the effective surface potential barrier, and secondly, the difference between the effective barriers for the two systems manifests itself more strongly for states at higher energies (closer to E_F).

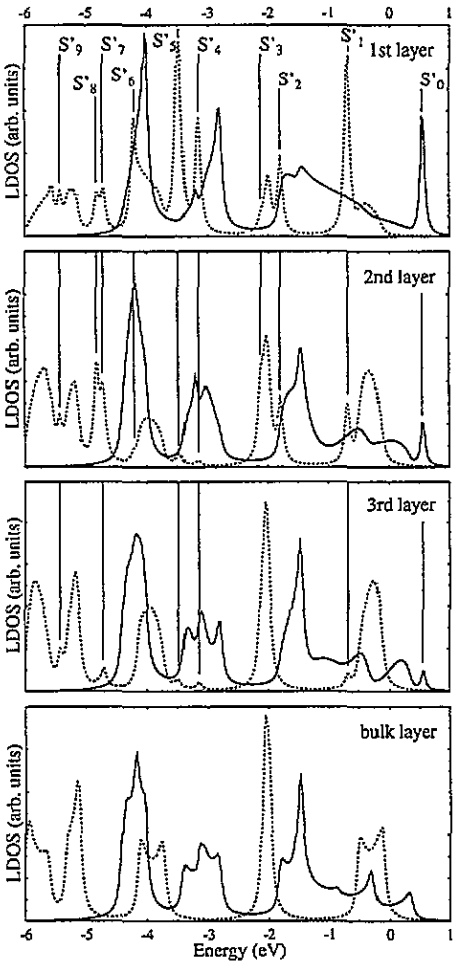

Figure 3. Layer-resolved density of states for clean Pt(111) for $k_\parallel$ at $\overline{\Gamma}$ (full curves) and $\overline{K}_{1\times1}$ (broken curves) for the three outermost Pt layers and a bulk layer. Surface states are denoted $S'_0, \ldots, S'_9$. In all panels, the LDOS scale is the same. The surface potential barrier was modelled by a reflecting step located 1.2 Å above the topmost internuclear plane.

5. Photoemission by circularly polarized light

As is well known (see, for example, Feder 1985 and references therein), for normally incident circularly polarized light, relativistic dipole selection rules imply that the spin-up and spin-down 'partial' normal photoemission intensities I_+ and I_- originate from initial states of double-group symmetry types Λ_6 and Λ_{4+5}, respectively. The spin polarization P of the photocurrent is related to these intensities by $P = (I_+ - I_-)/(I_+ + I_-)$.

For photon energy $\hbar\omega = 10.9\,\text{eV}$, let us first focus on the calculated normal emission spectra from clean Pt(111) (the second panel in figure 4). From the band structure panel it can be seen that the energies of the I_- and I_+ peaks at $-0.3\,\text{eV}$ and $-0.8\,\text{eV}$ coincide with the intersection points of Λ_{4+5} and Λ_6 initial-state bands with the Λ_6 final-state band (full circles) shifted downward by the photon energy. This identifies these spectral features as due to bulk interband transitions. The same interpretation applies to the two weak I_+ peaks

near −2.2 eV and −3.4 eV and the tiny I_- feature near −4.4 eV. Comparing (in the second panel of figure 4) the resulting calculated spin-averaged spectrum with its experimental counterpart (due to Schönhense *et al* 1985), we notice very good agreement with regard to the two dominant peaks and the weaker one near −3.4 eV.

For $\sqrt{3} \times \sqrt{3}$R30°-Xe/Pt(111) (the third panel of figure 4), the calculated spin-resolved spectra show again the 'clean-Pt' peaks at −0.3 eV, −0.8 eV and −3.4 eV. In addition, there are two small I_+ peaks, originating from initial states of symmetry type Λ_6, at −0.5 eV and −0.2 eV. From the band structure, the former peak can be associated with a direct transition between 'surface-umklapped' bands. The −0.2 eV peak is likely to arise from the interface state I_1 found in our surface LDOS (see figure 2). The absence of these two small features in the experimental spectrum may be understood from their sensitivity to details of the potential barrier between Pt and Xe. Choosing a more realistic barrier might, in particular, shift the calculated interface feature closer to the Fermi energy, where the experimental spectrum indeed exhibits a shoulder. The two sharp peaks at −4.9 eV and −4.5 eV originate from the $m_j = 1/2$ and $m_j = 3/2$ parts of the Xe $5p_{3/2}$ level, respectively, which we already encountered in the Xe layer density of states (see figure 2). The identification of the splitting mechanism as the lateral interaction within the Xe layer is further corroborated by the increase of the peak separation in the photoemission spectra for the closest-packed hexagonal Xe layer (see the bottom panel of figure 4). Since this layer is incommensurate with the substrate, the Xe/Pt system cannot be handled by our computer code, but the experimental spectrum in the Xe region is seen to be well reproduced already by our calculation for a stand-alone Xe layer. This agreement as well as our finding that for the commensurate Xe/Pt system the polarization of the Xe peaks reaches ±100% (the same as for Xe alone) are due to only very weak coupling of the adsorbate to the substrate. Further, the matching of the calculated Xe peak positions with experiment indicates the basic adequacy of our Xe potential. In figure 5 we present analogous results for the photon energy $\hbar\omega = 11.7$ eV, at which in addition emission from the Xe $5p_{1/2}$ level ($E = -6.0$ eV) becomes possible. For the two overlayer cases the photoemission spectra again faithfully reflect the Xe LDOS. In the Pt band region (see the upper panel of figure 5) we notice again the interface state feature at −0.2 eV, which is independent of the photon energy.

For both photon energies (see figures 4 and 5), there is however a significant discrepancy between theory and experiment with regard to the relative heights of the Xe-derived photoemission peaks: the Λ_{4+5} symmetry peak (associated with the $5p_{3/2}$ $m_j = 3/2$ level) is too strong in the calculated spectra. As possible reasons for this one might think of shortcomings in our Xe potential model, like the use of a bulk ion core potential or even the muffin-tin approximation itself. A more fundamental physical origin will become apparent when looking at the spin polarization, P, of the Xe features in photoemission from $\sqrt{3} \times \sqrt{3}$R30°-Xe/Pt(111) at the two photon energies (figure 6). In accordance with relativistic dipole selection rules we obtain $P = +1.0$ for the $5p_{1/2}$ peak, $P = +0.8$ for the $5p_{3/2}$ $m_j = 1/2$ peak and $P = -1.0$ for the $5p_{3/2}$ $m_j = 3/2$ peak, with the slight reduction of the second value being due to the lifetime broadening of the large neighbour peak. Comparison with experiment (Schönhense *et al* 1985) shows agreement with regard to the sign of P, but the measured absolute values are, firstly, substantially smaller and, secondly, depend strongly on the photon energy. This kind of discrepancy between theory and experiment is already known from photoemission studies on clean metal surfaces (Tamura *et al* 1989) and semi-infinite Xe(111) (Halilov *et al* 1993b): experimental spin-resolved intensity spectra exhibit opposite-spin features ('ghost peaks'), which are absent in the calculated spectra. As was suggested in those papers and substantiated by simplified

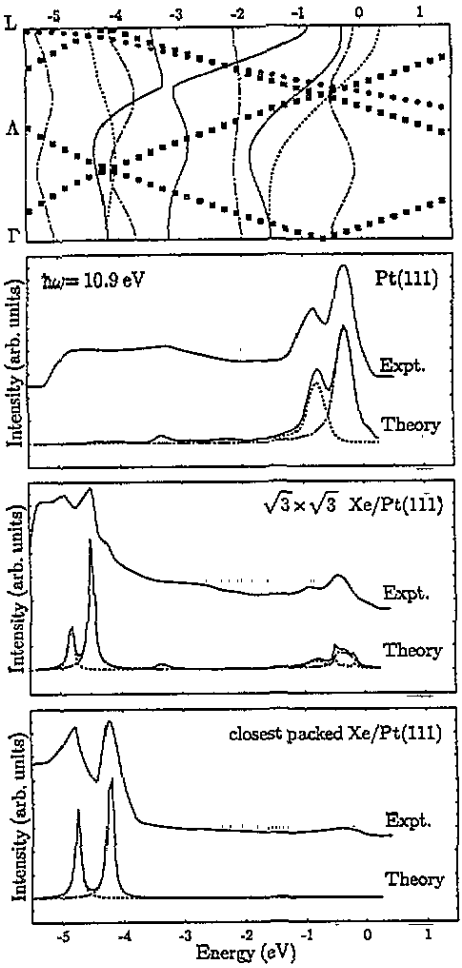

Figure 4. Experimental (Schönhense *et al* 1985) and theoretical normal photoemission intensities for normally incident circularly polarized 10.9 eV photons from clean Pt(111) (second panel), $\sqrt{3} \times \sqrt{3}$R30°-Xe/Pt(111) (third panel) and incommensurate closest-packed Xe/Pt(111) (bottom panel). In the latter case, the theoretical spectra were obtained for a 'stand-alone' Xe layer. The spin-averaged theoretical spectra (full curves) are resolved into spin-up (Λ_6) (dotted curves) and spin-down (Λ_{4+5}) (chain curves) contributions. For interpreting the spectra, the bulk band structure of Pt is shown (top panel) for initial-state bands along Γ–Λ–L (full and broken curves) and backfolded from the $\overline{K}_{1\times1}$-points (chain curves) together with the fully symmetric Λ_6 final-state bands, shifted downwards by the photon energy 10.9 eV, along Γ–Λ–L (full circles) and backfolded from the $\overline{K}_{1\times1}$-points (full squares).

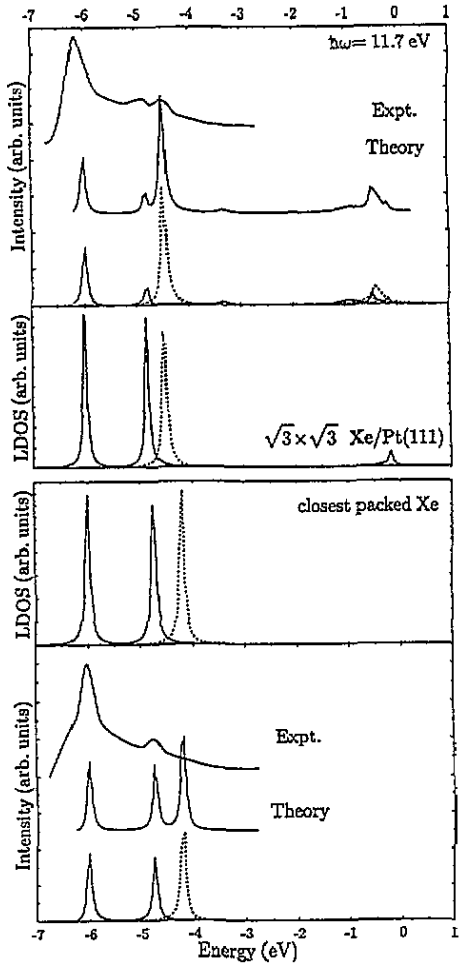

Figure 5. Experimental (Schönhense *et al* 1985) and theoretical normal photoemission intensities for normally incident circularly polarized 11.7 eV photons from $\sqrt{3} \times \sqrt{3}$R30°-Xe/Pt(111) with FCC-type ($\cdots ABCA$) stacking of the Xe layer (top panel) and the incommensurate Xe/Pt(111) system with a hexagonally closest-packed Xe layer (bottom panel). In the latter case, the theoretical spectra were obtained for a 'stand-alone' Xe layer. In both panels, the spin-averaged theoretical spectra (central curves) are resolved into spin-up (Λ_6) and spin-down (Λ_{4+5}) contributions (bottom curves). The two centre panels show the corresponding densities of states of the Xe layer as resolved with respect to the symmetry types Λ_6 (full curves) and Λ_{4+5} (broken curves).

model calculations (Stolle 1992), they originate from excitation channels involving electron–hole scattering processes, which are not taken into account in present-day one-step model

photoemission formalisms. For rare gas adsorbate systems, the importance of such Auger-type processes in spin-resolved photoemission has been convincingly demonstrated by 'sub-threshold' experimental data (Schönhense *et al* 1986, Heinzmann 1990 and references therein). Formally speaking, they correspond to higher-order Keldysh diagrams, which are not yet included in our theory.

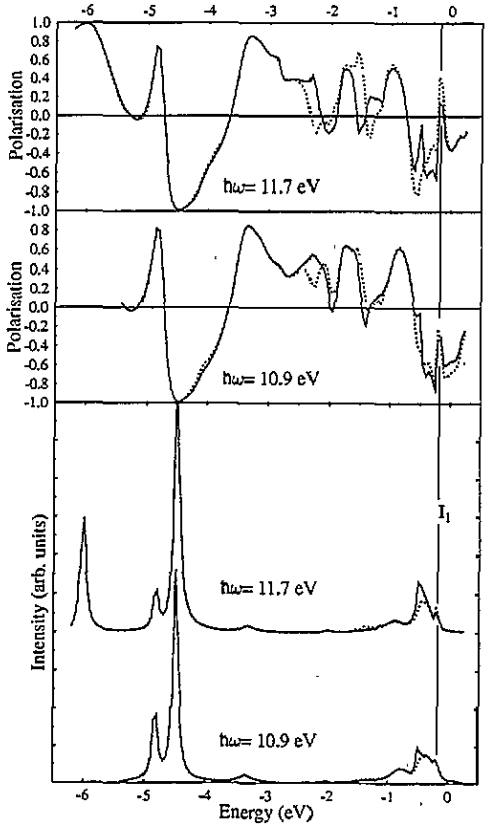

Figure 6. Theoretical normal photoemission intensities (lower panel) and electron spin polarization (upper panels) from $\sqrt{3} \times \sqrt{3}$R30°-Xe/Pt(111) for normally incident circularly polarized light of 10.9 eV and 11.7 eV photon energy, for FCC-type ($\cdots ABCA$, full curves) and HCP-type ($\cdots ABCB$, broken curves) stacking order of the Xe overlayer. The interface state I_1 is marked by a vertical thin full line.

To see the influence of the lateral position of the Xe overlayer relative to the substrate on photoemission from $\sqrt{3} \times \sqrt{3}$R30°-Xe/Pt(111), we compare in figure 6 spin-averaged intensity and spin polarization spectra produced by circularly polarized light for the FCC-type ($\cdots ABCA$) and HCP-type ($\cdots ABCB$) stacking cases of the adsorbate layer. As one would expect because of the very weak coupling of Xe to the substrate, practically no difference between the two cases shows up in the Xe spectral region. However, the interface state peak at −0.2 eV and the Pt interband transition feature around −0.4 eV depend noticeably on the assumed stacking order. Comparing the Pt intensity peak with its experimental counterpart (see figure 4), the HCP-type stacking seems to be favoured. The difference for the two stackings is strongest in the spin polarization spectra for $\hbar\omega = 11.7$ eV (see the top panel

of figure 6). In particular, P at the interface state energy is more than twice as large for the HCP-type than for the FCC-type stacking order of the Xe layer.

6. Photoemission by linearly polarized light

While spin-resolved photoemission studies from non-magnetic systems traditionally employed circularly polarized radiation, two new photoelectron spin polarization effects were recently discovered to occur in normal emission for linearly polarized and even unpolarized light. Firstly, for normal incidence of linearly polarized light on surfaces with a threefold rotation axis (parallel to the surface normal), spin polarization was theoretically predicted by Tamura *et al* (1987) and verified experimentally by Schmiedeskamp *et al* (1988). The surface sensitivity of this effect was exploited in an investigation of the Au/Pt overlayer system by Stoppmanns *et al* (1991). Secondly, a more general spin polarization effect, not restricted to threefold symmetry, was found theoretically by Tamura and Feder (1991a, b) and experimentally by Schmiedeskamp *et al* (1991) for off-normally incident p-polarized and even unpolarized light. While both effects owe their existence to the breaking of translation symmetry normal to the surface (and are absent in the three-step model of photoemission involving infinite-bulk interband transitions), the underlying physical mechanisms are quite different. The first effect is due to a time-reversal peculiarity of the basis functions of the double group Λ_{4+5} and can only arise from initial states of this symmetry type. The second effect is (in the case of threefold rotation symmetry) associated with the spin–orbit-induced hybridization of wavefunctions of (single-group) spatial symmetries Λ^1 and Λ^3 in double-group symmetry Λ_6 states. For threefold surfaces, the different azimuthal rotation behaviour of the two effects allows, in a single experiment, their separate observation: as in-surface-plane spin polarization components P_x and P_y, respectively (Tamura and Feder 1991a). In view of their surface and interface sensitivity, we have explored the two effects for the present Xe/Pt overlayer system.

In figure 7, we present results for the above-used photon energy $\hbar\omega = 11.7\,\text{eV}$. For s-polarized light, the photoemission intensity spectra are found, in accordance with symmetry arguments, to be identical to the ones produced by circularly polarized light. The in-plane spin polarization P_y is identically zero for a stand-alone Xe layer because of its sixfold symmetry. For clean Pt, several P_y features with values up to 20% are seen (see the top panel of figure 7). While the features below $-3.5\,\text{eV}$ and above $-0.5\,\text{eV}$ are clearly related to intensity peaks arising from Λ_{4+5} initial states, in accordance with the above-stated nature of this spin polarization effect, the negative P_y peak around $-1.4\,\text{eV}$ has no visible counterpart in the intensity spectrum. However, as can be seen from the band structure (figure 4), there is a flat Λ_{4+5} band in this energy range, i.e. a very high density of states. The latter thus manifests itself clearly in the polarization but not in the intensity spectrum, demonstrating once again the already well known higher sensitivity of polarization analysis. For Xe/Pt(111), the P_y features found on clean Pt below $-3.5\,\text{eV}$ are weakened, but above $-2.5\,\text{eV}$ new P_y peaks occur, which strongly depend on the lateral position (FCC- or HCP-type stacking) of the commensurate Xe layer relative to the substrate. The maximum $P_y = 0.2$ at $-0.4\,\text{eV}$ in the FCC stacking case is seen to be associated with an intensity maximum, which we earlier already interpreted (on the grounds of the band structure shown in the top panel of figure 4) as due to a direct transition from 'surface-umklapped' initial states. For HCP stacking, P_y is almost zero in this energy range. The large negative P_y peaks obtained in the FCC stacking case around $-2.0\,\text{eV}$ and $-1.5\,\text{eV}$ appear to have no counterparts in the intensity spectrum. From the band structure, however, direct transitions from the flat

umklapped initial-state band around −2 eV, which is degenerate with respect to Λ_6 and Λ_{4+5}, are possible. The feature around −1.5 eV can be understood as a modification of the feature already found on clean Pt(111). For HCP stacking, we note again drastic changes in P_y. In particular, the peak around −1.5 eV has changed its sign and a new positive peak occurs around −2.3 eV. We associate the latter with the Pt surface state S_3 in our layer-resolved density of states (Fig.2). This interpretation will be corroborated by the observation of a small intensity peak at this energy for photon energy 21.2 eV (see below).

For p-polarized light with $\hbar\omega = 11.7$ eV, the clean Pt(111) intensity spectrum (bottom panel of figure 7) shows the same peaks as in the s-polarized case, but the peaks from Λ_6 initial states are enhanced, since selection rules now also allow contributions from the Λ_6^1 spatial parts of the Λ_6 states. This is particularly striking for the peak at −2.5 eV. Since the corresponding initial state is almost exclusively of Λ_6^1 character, the spin polarization P_x, which requires for its existence a Λ_6^1–Λ_6^3 hybrid (as we recalled above), should be close to zero. The calculated spectra confirm this. In contrast, the Λ_6-derived peaks around −0.8 eV and −3.4 eV are associated with sizable spin polarization (up to 30%). For Xe/Pt(111) with FCC-type stacking order, the intensity spectra by p-polarized light exhibit similar enhancements of Λ_6 features, most notably for the Xe peak at −4.8 eV and

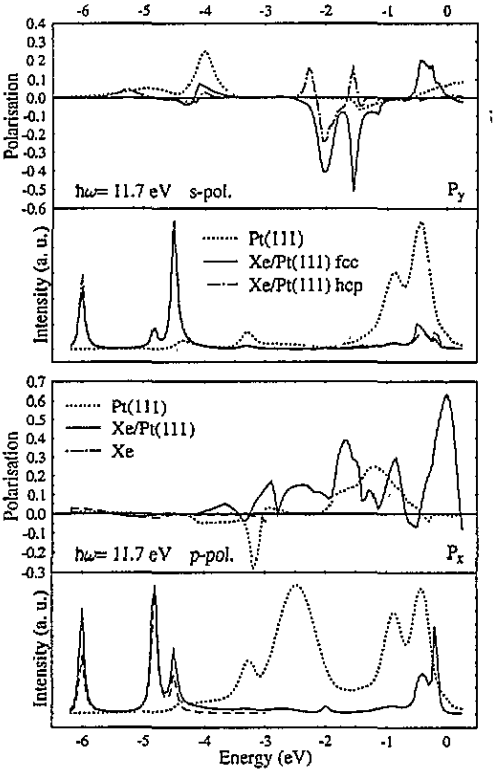

Figure 7. Theoretical normal photoemission intensity and spin polarization from clean Pt(111) and $\sqrt{3} \times \sqrt{3}$R30°-Xe/Pt(111) with FCC- and HCP-type stacking order by 11.7 eV *linearly polarized light* incident in the yz plane at 45° to the surface normal. Upper two panels: spin polarization (component P_y) and spin-averaged intensities for s-polarized light. Lower two panels: spin polarization (component P_x) and spin-averaged intensities for p-polarized light for clean Pt, Xe/Pt with FCC-type stacking and for a 'stand-alone' Xe monolayer.

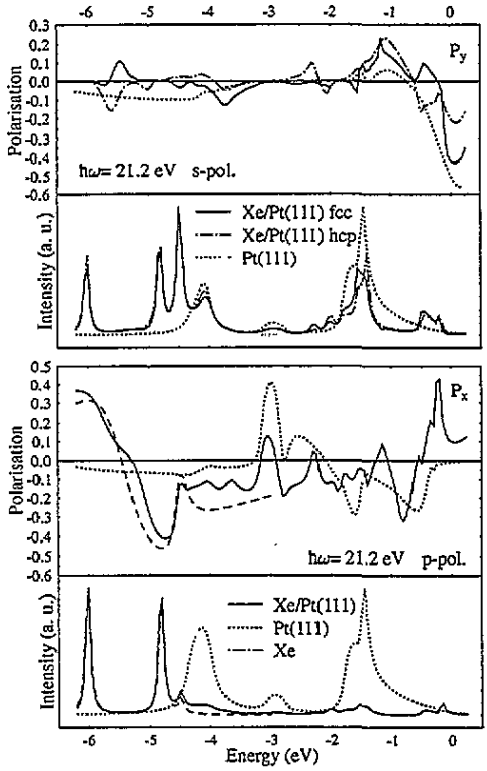

Figure 8. Photoemission by *linearly polarized light*: as figure 7, but for photon energy 21.2 eV.

the interface state peak at −0.2 eV. Around the latter, we note a 60% polarization peak. For HCP-type stacking order (not shown), the P_x spectra are modified in a discernible but relatively minor way.

The new spin polarization effects produced by linearly polarized light are further illustrated by spectra calculated for a higher photon energy (21.2 eV, see figure 8). As their interpretation is to a large extent similar to those for $\hbar\omega = 11.7$ eV, it may suffice to point out some salient aspects and differences. For FCC-stacked Xe/Pt(111) with s-polarized light, the P_y spectrum (top panel of figure 8), which requires Λ_{4+5} initial states, shows a distinct peak at −5.5 eV, i.e. about halfway between the two Λ_6 Xe intensity peaks. Together with the hardly visible broad intensity peak around −5.2 eV, this P_y peak can, with the aid of the band structure (figure 4), be traced back to a direct transition originating from a (lifetime-broadened) surface-umklapped initial state. For HCP-type stacking, P_y is seen to change sign, with a sizable peak around −5.7 eV. A new intensity peak occurs at −2.3 eV. From our layer-resolved density of states (figure 2), it can be understood to arise from the Pt surface state S_3. In the P_y spectra, we note at this energy a distinct peak in the HCP-type stacking case and almost zero in the FCC-type stacking case, similar to our above finding for $\hbar\omega = 11.7$ eV. For p-polarized light, P_x shows, at the same energy, a sizable peak relative to the −13% base line. In contrast to the $\hbar\omega = 11.7$ eV results, P_x below about −4.5 eV is now very strong with maxima up to ±40% associated with the two Λ_6 Xe peaks, with little difference between Xe/Pt(111) and the stand-alone Xe layer. While the P_y effect must always vanish for the single Xe layer because of its sixfold rotation symmetry, we thus see that the actual size of P_x strongly depends on the photon energy.

Since the initial states are the same, this means a strong dependence on the final states and the transition matrix elements.

7. Concluding remarks

The application of our relativistic layer density of states (LDOS) and photoemission theory to the commensurate adsorbate system $\sqrt{3} \times \sqrt{3}$R30°-Xe/Pt(111) has revealed a remarkable asymmetry between the influence of adsorbate and substrate on each other. While the Xe-5p-derived features in LDOS and photoemission for Xe/Pt are practically the same as for a hypothetical stand-alone Xe layer, a wealth of new Pt-derived features is produced by 'surface umklapp' (by a surface reciprocal lattice vector): firstly, a number of electronic states localized in the two topmost Pt layers and secondly, features in the photoemission intensity and spin polarization spectra, which can be understood in terms of direct transitions originating from umklapped bulk Pt bands. These latter features are only weakly visible in the (spin-averaged) intensity but are increasingly visible in the spin polarization produced by circularly and linearly polarized light. Changes in the assumed lateral position of the Xe layer (FCC- against HCP-type stacking) and the parameters describing the interface potential barrier manifest themselves most strongly in the spin polarization spectra obtained with linearly s-polarized light. Such high surface sensitivity of the 'new spin polarization effect' is plausible from the vital role of the surface in producing this effect, and has been found earlier for clean metal surfaces (Tamura and Feder 1991a, b) and a metal–metal adsorbate system (Stoppmanns *et al* 1991). An experimental investigation of this effect for Xe/Pt therefore appears to be very worthwhile in view of obtaining, via a comparison with our calculated spectra, more precise information on the adsorption geometry and a more refined model for the Xe–Pt interface potential barrier.

Concerning the observability of the electronic states localized in the surface region, those at energies below -4 eV are very difficult to see in photoemission because of the strong lifetime broadening. However, those closer to the Fermi energy, especially an interface state residing in the Xe and in the topmost Pt layer, manifest themselves in photoemission, most clearly so in the spin polarization spectra.

For the three Xe-5p-derived features, our calculated results agree very well with experimental data (see Heinzmann 1990, and references therein) with regard to the existence, energy position and sign of the spin polarization produced by circularly polarized light. However, there remain significant discrepancies in relative intensity peak heights and, in particular, in the absolute values of the spin polarization. The latter are much smaller in experiment and, furthermore, strongly depend on the photon energy, in contrast to our calculations. We ascribe these discrepancies to the same kind of underlying physical mechanism as the experimentally observed but theoretically absent 'opposite-spin peaks' (ghost peaks) for clean metal surfaces (Tamura *et al* 1989) and semi-infinite Xe(111) (Halilov *et al* 1993b): Auger-like electron–hole scattering processes, which provide additional excitation channels interfering with the simple electric dipole excitation channel. These processes are not included in present-day one-step model photoemission formalisms. Our above findings for Xe/Pt(111) strongly emphasize the importance of these processes and the need for further development of photoemission theory.

Acknowledgments

This work was funded by the German Ministry for Research and Technology under

contract no. 055PGABB7. The numerical calculations were performed on the NEC SX-3 supercomputer of the Land NRW (project number P047). Further, it is our pleasure to thank E Tamura for his valuable advice and help in implementing some generalizations of the relativistic photoemission and LDOS computer codes.

References

Ackermann B and Feder R 1985 *J. Phys. C: Solid State Phys.* **18** 1093
Di W, Smith K E and Kevan S D 1992 *Phys. Rev.* B **45** 3652
Feder R 1978 *Solid State Commun.* **28** 27
—— (ed) 1985 *Polarized Electrons in Surface Physics* (Singapore: World Scientific)
Halilov S V, Tamura E, Gollisch H, Meinert D and Feder R 1993a *J. Phys.: Condens. Matter* **5** 3859
Halilov S V, Tamura E, Gollisch H, Feder R, Kessler B, Müller N and Heinzmann U 1993b *J. Phys.: Condens. Matter* **5** 3851
Hedin L and Lundqvist BI 1971 *J. Phys. C: Solid State Phys.* **4** 2064
Heinzmann U 1990 *Photoemission and Absorption Spectroscopy of Solids and Interfaces with Synchrotron Radiation* ed M Campagna and R Rosei) (Amsterdam: North-Holland)
Hilgers G, Potthoff M, Wirth S, Müller N, Heinzmann U, Haunert L, Braun J and Borstel G 1991 *Surf. Sci.* **252/252** 612
Kessler B, Müller N, Schmiedeskamp B, Vogt B and Heinzmann U 1990 *Phys. Scr.* **41** 953
Kirschner J 1985 *Polarized Electrons at Surfaces (Springer Tracts in Modern Physics* **106***)* (Berlin: Springer)
Potthoff M 1991 *Diplomarbeit* Universität Bielefeld
Scheffler M, Horn K, Bradshaw A M and Kambe K 1979 *Surf. Sci.* **80** 69
Schmiedeskamp B, Vogt B and Heinzmann U 1988 *Phys. Rev. Lett.* **60** 651
Schmiedeskamp B, Irmer N, David R and Heinzmann U 1991 *Appl. Phys.* A **53** 418
Schneider C M, Garbe J, Bethke K and Kirschner J 1989 *Phys. Rev.* B **39** 1031
Schönhense G, Eyers A, Friess U, Schäfers F and Heinzmann U 1985 *Phys. Rev. Lett.* **54** 547
Schönhense G, Eyers A and Heinzmann U 1986 *Phys. Rev. Lett.* **56** 512
Stolle T 1992 *Diplomarbeit* Universität Duisburg
Stoppmanns P, Heidemann B, Irmer N, Müller N, Vogt B, Schmiedeskamp B, Heinzmann U, Tamura E and Feder R 1991 *Phys. Rev. Lett.* **66** 2645
Tamura E, Piepke W and Feder R 1987 *Phys. Rev. Lett.* **59** 934
Tamura E and Feder R 1989 *Solid State Commun.* **70** 205
—— 1991a *Solid State Commun.* **79** 989
—— 1991b *Europhys. Lett.* **16** 695
Tamura E, Feder R, Vogt B, Schmiedeskamp B and Heinzmann U 1989 Z. *Phys.* B **77** 129
von Barth U and Hedin L 1972 *J. Phys. C: Solid State Phys.* **5** 1629
Waclawski B J and Herbst J F 1975 *Phys. Rev. Lett.* **35** 1594